Stability of ultrathin nanocomposite polymer films controlled by the embedding of gold nanoparticles

George Amarandei[1], Ian Clancy[1], Colm O'Dwyer[1,2], Arousian Arshak[1] and David Corcoran[1]*

[1]Department of Physics and Energy, University of Limerick, Limerick, Ireland

[2]Department of Chemistry, University College Cork, Cork, Ireland

KEYWORDS. thin polymer films, nanoparticles, dewetting, embedding.

ABSTRACT. Thin and ultra-thin polymer films combined with nanoparticles (NPs) are of significant interest as they are used in a host of industrial applications. In this paper we describe the stability of such films ($h_{poly} \leq 30$ nm) to dewetting; specifically how the development of a spinodal instability in a composite NP-polymer layer is controlled by the embedding of Au NPs. At working temperatures (T = 170 °C) above the polymer glass transition temperature ($T_g \approx 100$ °C) the absence of Au NPs leads to film rupture by nucleation dewetting while their presence over a large surface area enhances the development of a spinodal instability without destroying the film continuity. When the NPs embed the surface undulations are suppressed. The dynamics change from an unstable to a stable state and the thin composite NP-polymer layer returns to a flat configuration while the wavelength of the pattern remains constant. Moreover, we demonstrate from a thermodynamic perspective that NPs will remain on the surface or embed in

the polymer film depending on their free energy which is determined by the NP interactions with the underlying polymer, the native SiO_x layer and the Si substrate.

INTRODUCTION

The stability of pristine thin polymer films[1–3] and composites, where the polymer film is combined with metal/dielectric nanoparticles[4–6] or with thin continuous metal/dielectric layers,[7–9] is studied as it has direct application to coatings, adhesives and electronics.[4,5,10–12] Thin polymer films covered by nanoparticles represent an intermediate case between pristine thin polymer films[1–3] and capped films[7–9] i.e. films covered by continuous solid layers. There has been increased interest in this intermediate case recently as nanoparticles (NPs) positioned on polymer surfaces (or within polymer films) can modify local polymer structure.[13,14] Thus, the presence of NPs can lead to unique electrical, mechanical, optical sensing, catalytic sensing, and antimicrobial properties that can be tuned by varying the NP size, shape, type, and/or surface functionality.[15–17] Despite the number of applications, understanding of the dynamics of thin or ultra-thin nanocomposite layers is still in its infancy when compared to pristine polymer films. Hence, their dynamics can be described only in a limited sense by adjusting the existing theoretical framework for pristine-polymer film dynamics to include new terms reflecting additional interactions.

In this paper we investigate the stability against dewetting of ultra-thin polystyrene films (25 nm $\leq h_{poly} \leq$ 30 nm) covered by metal nanoparticles. Also, the work aims to emphasize the role of nanoparticle-substrate interactions during nanoparticle embedding. These aspects were not previously considered in the literature mainly because the vast majority of the experiments were

performed on relatively thick films (100 nm ≤ h_{poly} ≤ 500 nm) of polymers and/or with larger molecular weight.[6–17]

In general, the stability against dewetting for Au NP-covered thin polymer films can be predicted by the total interaction potential between the air-polymer and polymer-substrate interfaces. In a previous paper,[18] we have shown that the total potential Φ controlling the system stability is a combination of the van der Waals interaction between the two polymer interfaces $\Phi_{poly}(h_{poly})$ and the interaction between the Au NPs with a mean radius R_p and the underlying layers $\Phi_{AuNP}(h_{poly}, R_p)$. The influence of each term is weighted by the changes in the amount of Au present at the air-polymer interface i.e. $\Phi = (1 - C_f)\Phi_{poly}(h_{poly}) + p_d\Phi_{AuNP}(h_{poly}, R_p)$, where C_f and p_d represent the fractional coverage and the number particle density, respectively. When no Au is present $\Phi = \Phi_{poly}(h_{poly})$, the film becomes metastable (e.g. polystyrene films with thicknesses larger than 20 nm are known to be metastable on Si substrates covered by a native oxide layer[1–3]) and it dewets via nucleation. For low coverage and particle density the $\Phi_{poly}(h_{poly})$ dominates and the film remains metastable.[18] When Au is present and the C_f and p_d are above a certain threshold the $\Phi_{AuNP}(h_{poly}, R_p)$ term becomes dominant. The system is unstable and able to develop a spinodal instability that patterns the polymer film.[18] The change in the amount of Au was governed by the NP aggregation[18] and the existence of a thin capping layer (created by the interconnected NPs through bridging chains) was hypothesized. The pattern wavelength increases with heating time and it is also accompanied by a similar increase in roughness.[18, 19] However, once the coverage decreases and the distance between particles becomes larger than the connectivity limit between them, the film becomes flat.[18,19]

Based on these previous studies, we expect for the particular case of ultra-thin polystyrene films (25 nm ≤ h_{poly} ≤ 30 nm) covered by a Au layer with nominal thickness of 1 nm presented

here that a spinodal instability should develop as the initial coverage is above the critical threshold.[18] Indeed, this phenomenon takes place. However, in the current work the film and the pattern dynamics differ from the previous cases investigated as the Au NPs do not remain at the film surface, but embed in the film. This embedding only leads to changes in the pattern roughness while the wavelength remains constant.

EXPERIMENTAL METHODS

Ultra-thin polysterene [PS10, M_w = 10 kg/mol, R_g = 2.59 nm, M_w/M_n = 1.05, Sigma-Aldrich, UK] films were obtained by spin coating from 2 – 3% (w/w) polymer solution in toluene onto Si substrates (with native oxide, $h_{SiOx} \simeq 2.0$ nm) with a resistivity of 2 – 3 Ω cm. Ultra-thin PS10 films with thicknesses of 25, 26, 28 and 30 nm were obtained (see **Figure S1** in *Supp. Inf.*). Prior to spin coating the Si substrates were cleaned in a jet of CO_2 ice crystals. Au layers with nominal thickness of 1 nm were then sputtered at a low rate (0.09 nm s^{-1}) onto the polymer thin films creating a Si/SiO_x/Polymer/AuNP/Air configuration (further details in *Supp. Inf.*).[18–21] The deposition led to uniformly distributed NPs (**Figure 1a**) on the polymer surface in the central region of the samples (see **Figure S2**) allowing a direct comparison between Si/SiO_x/Polymer/Air (**Figure 1b**) and Si/SiO_x/Polymer/AuNP/Air regions (**Figure 1c-g**). The mean radius value of the NPs was $R_p \approx 1.55$ nm and the fractional Au coverage was $C_f \approx 0.14$. The same Au spatial distribution, fractional coverage and particle size was obtained for all samples, independent of the polymer film thickness.

The sample with thickness of h_{PS10} = 25 nm was repeatedly heated, removed, cooled and analysed for several heating intervals of increasing duration, starting at t = 1440 min up to a total heating time of 37440 min (**Figure 1**). The change in roughness and wavelength was monitored

and recorded (see **Figure 2a**). As the wavelength remained constant throughout the experiment, the samples with polymer thicknesses of 26, 28 and 30 nm were expected to exhibit similar behaviour and were extracted after single heating time steps i.e. 4320, 10080 and 20160 min, respectively (**Figure 2b**). All experiments were performed in a closed air environment in an oven at 170 ºC.

Au atoms are expected to embed within the polymer matrix as a result of the sputter deposition, but, for the deposition parameters used here (see Supp. Inf.), the amount of Au implanted below the interface will be smaller than 0.1 of a monolayer (see Ref. 11 and 18 for further details). Moreover, once above the glass transition temperature, these atoms are the first to diffuse and aggregate with the larger Au clusters/NP due to their large diffusion coefficient.[18]

Optical imaging and roughness measurements were performed using a MicroPhase camera (PhaseView, France) placed on a Zeiss AxioImager A1.m microscope. The MicroPhase camera allows 3D visualization with highly repeatable non-contact optical surface profiling capabilities. Roughness, R, is the root mean square average of polymer height deviations and was calculated using $R = \sqrt{\sum_i \left(h_i - \bar{h}\right)^2 \Big/ N}$, where $\left(h_i - \bar{h}\right)$ is the local deviation of film height from the average value and N is the number of points where the height is measured. In this work a normalized roughness measure is used.[18,19] In **Figure 2a** the roughness value measured for each time step is normalized to the mean value for all time steps**.** In **Figure 2b** the normalization is performed relative to the mean value of the roughness of the four samples.

The initial (t = 0 min) Au NP distributions were imaged using electron microscopy[18] and X-ray photoelectron spectroscopy (XPS). These methods allow the measurement of the concentration of Au present at the surface and the characterisation of possible polymer surface degradation during the heating steps.[12] Angle-resolved XPS was carried out to get an insight into the location

of the Au NPs.[22] By tilting the sample relative to normal, the measurements were made more surface sensitive, i.e. as the take-off angle decreases, the sampling depth decreases and near surface regions are probed.

RESULTS

Heating a thin polystyrene film (h_{PS10} = 25 nm) at 170 ºC for t = 1440 min allows for nucleation dewetting development[1,18] in the uncovered polymer region (i.e. for Si/SiO_x/Polymer/Air). This permits a disordered pattern to emerge and to rupture the continuity of the polymer film (**Figure 1b**). In contrast, in the Au NP covered region of the same sample (i.e Si/SiO_x/Polymer/AuNP/Air) an ordered pattern corresponding to a spinodal instability development perturbs the thin polymer films (**Figure 1c-f**). Further heating does not lead to significant changes in the nucleation dewetting pattern. In the Si/SiO_x/Polymer/AuNP/Air region the roughness of the ordered pattern decreases with time (**Figure 2a**) as the surface undulations initiated by the instability are almost suppressed by t = 37440 min (**Figure** 1f). Prolonged heating periods do not affect the pattern wavelength for a polymer thickness of h_{PS10} = 25 nm (**Figure 1 c-g**). This result differs from previous findings[18] for polystyrene films with thicknesses in the range 44–26 nm covered by gold layers with nominal thicknesses of 1–3 nm, respectively. In those cases the pattern wavelength increases with the heating time.[18] The difference arises from the NP embedding that occurs in the samples studied here. In the earlier work[18,19] NP embedding was not observed, but NP surface aggregation was present. This difference is discussed later in this paper.

Starting with the same initial (t = 0 min) nanoparticle size and density the wavelength does increase as the polymer film thickness increases (see **Figure 2b**). The wavelengths for h_{PS10} = 26,

28, 30 nm were measured for 4320, 10070 and 20160 min. A decrease of the roughness in time can be inferred from these samples (**Figure 2b**) if one considers that roughness has a similar evolution for all film thicknesses. Indeed, at similar heating times, the amplitude of the pattern (as reflected by the roughness) for the h_{PS10} = 25 nm sample decreases (see **Figure 1** and **2a**).

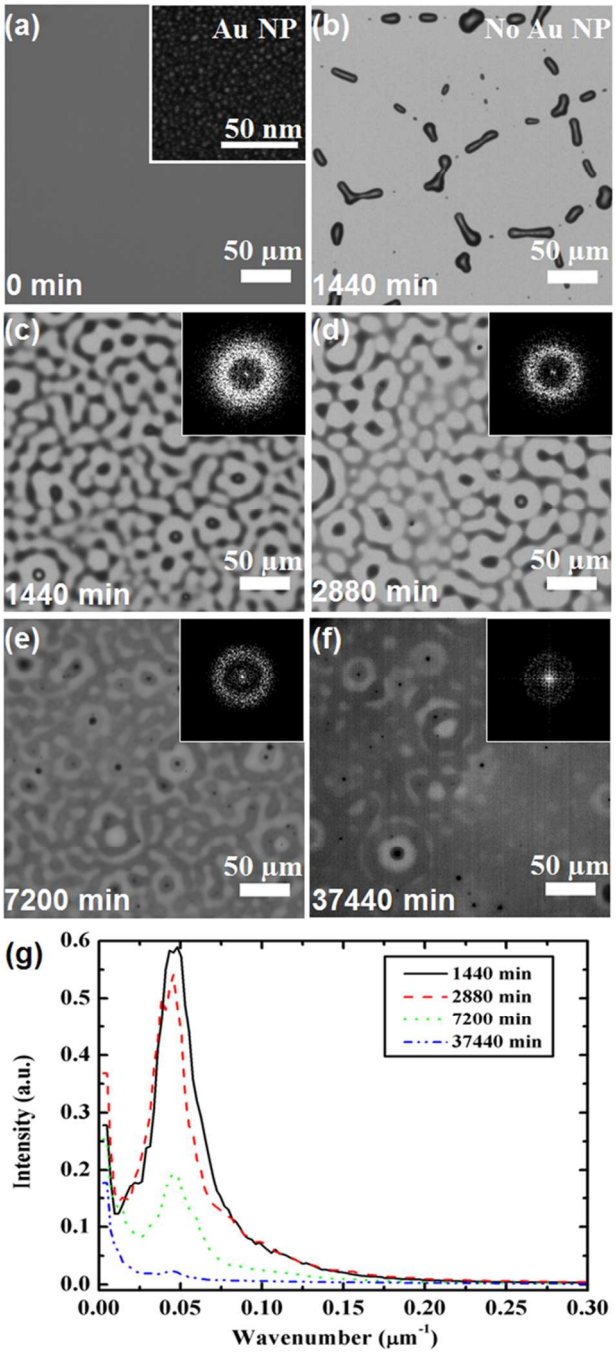

Figure 1. (a) Optical micrograph of the PS10 film (h_{PS10} = 25 nm) at t = 0 min. No significant differences were observed between the regions with and without Au NPs. The SEM inset shows the Au NPs as deposited (nominal thickness of the Au layer is 1 nm). (b) The film rupture due to nucleation dewetting is fully developed in the region without Au at t = 1440 min. (c) – (f) The pattern developed in the Si/SiO_x/Polymer/AuNP/Air region of polymer film and its 2D FFT at different heating times (c) 1440 min, (d) 2880 min, (e) 7200 min and (f) 37440 min. (g) The FFT profiles show that the wavelength of the instability does not change with heating time.

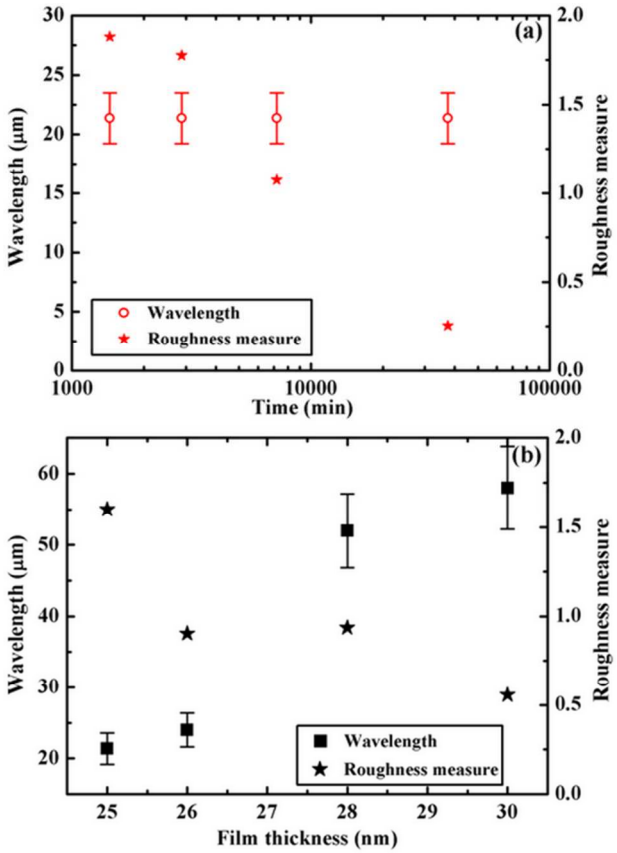

Figure 2. Wavelength and roughness evolution as function of (a) time for h_{PS10} = 25 nm and (b) film thickness. Wavelength and roughness values in (b) were acquired at heating times t = 1440, 4320, 10080 and 20160 min, from left to right, respectively.

We conclude that a spinodal instability pattern develops in heated ultra-thin PS regions covered by Au NPs; the wavelength of the pattern is polymer thickness dependent but it is also time independent. With prolonged heating a stabilizing effect occurs on the film and the roughness decreases with time. Extrapolation of this decrease leads to a flat film.

To understand this stabilization process we monitor the Au NP position in the films with thicknesses (25, 26 and 28 nm) at different times (1440, 4320 and 10080 min, respectively) using XPS. The intensity of the Au 4f peak (from a depth of ~ 4.7 nm from the air-polymer interface) is maximum at the beginning of the experiments (t = 0 min) when the Au nanoparticles are present at the film surface [see also Ref. 18]. With heating the intensity decreases and almost vanishes by t = 10080 min (see **Figure 3a**). The decrease in Au present at the air-polymer interface is confirmed by the changes in Au concentration from the survey spectra (**Table 1**). There are two processes previously reported in the literature that can lead to this decrease: particle aggregation[6,17–19]and/or their embedding in the film.[17,22–24] The complete embedding of a NP into a polymer melt is expected if $\gamma_1 > \gamma_{12} + \gamma_2$, where γ_1 and γ_2 are the surface energies of the NP and polymer, respectively, and γ_{12} is the NP-polymer interfacial energy.[25,26] This condition is satisfied for metal NPs on a polymer and, therefore, complete embedding is expected. However, the embedding does not always occur (as previously reported for experimental studies of Au NPs on polymers deposited by sputtering or thermal evaporation[18–21]). If the particles are embedded they can create a layer underneath the surface where the NPs can remain homogenously distributed.[25,26] For polystyrene films the Au NP diffusion below the film surface proceeds with the formation of a wetting layer (1.3 – 1.8 nm).[17] This layer covers the NP and creates a capillary pressure responsible for pushing the NP into the soft substrate

until the NP is fully submerged.[17] Once under the surface the particles can diffuse and aggregate.[17]

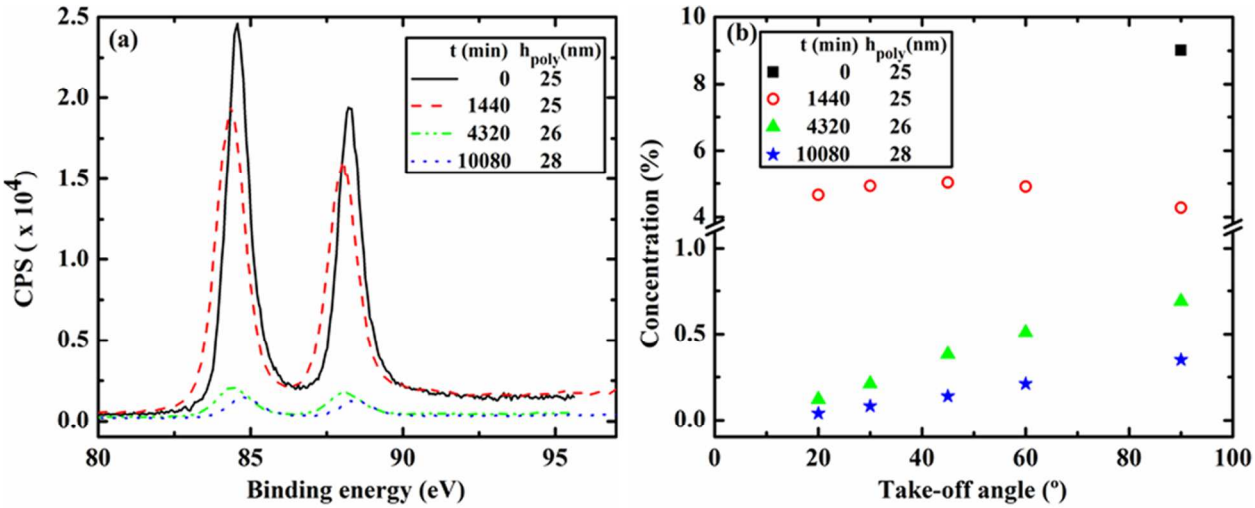

Figure 3. (a) Au 4f photo-electron spectrum at different times and for polymer thicknesses (25, 25, 26 and 28 nm top to bottom) at normal incidence; (b) Quantification of Au concentrations obtained using angle resolved XPS survey spectra. For t = 0 min, where the particles are at the film surface only the concentration obtained from normal emission spectrum (or take-off angle of 90º) is presented. Using an Inelastic Mean Free Path of 1.578 nm for Au (Quases software), the estimated analysis depth varied from ~1.6 nm to ~4.7 nm for a change in take-off angle from 20º to 90º.

Table 1. Chemical component concentration and energy from the survey spectra for different heating times and polymer film thicknesses.

	t = 0 min		t = 1440 min		t = 4320 min		t = 10080 min	
Name	**Energy** (eV)	**Conc.** (%)	**Energy** (eV)	**Conc.** (%)	**Energy** (eV)	**Conc.** (%)	**Energy** (eV)	**Conc.** (%)
C1s	284.6	78.1	284.1	53.3	284.4	94.4	284.6	97.1
O1s	532.6	12.2	532.1	28.7	532.4	4.9	532.6	2.6
Au 4f	84.6	9.0	84.1	4.5	84.4	0.7	84.1	0.3
Si 2s	–	–	152.1	13.5	–	–	–	–

The polymer film thicknesses are 25, 25, 26 and 28 nm. Due to the low resolution of the survey spectrum the Au 4f is seen as a single peak.

Table 2. Chemical assignments from the high resolution spectrum C1s signal

	t = 0 min		t = 1440 min		t = 4320 min		t = 10080 min	
Name	**Energy** (eV)	**Conc.** (%)	**Energy** (eV)	**Conc.** (%)	**Energy** (eV)	**Conc.** (%)	**Energy** (eV)	**Conc.** (%)
C – C, C – H	284.8	84.2	284.8	56.3	284.5	89.7	284.8	89.0
C – OR, C – OH	286.0	9.8	286.3	28.3	285.6	5.8	286.0	2.8
C = O	287.3	1.8	–	–	–	–	–	–
O – C = O	288.8	1.7	289.0	7.4	–	–	–	–
$\pi \rightarrow \pi^*$	291.6	2.5	291.4	8.0	291.36	4.5	291.4	7.3
							295.4	0.9

The assignments correspond to the data presented in **Table 1**. The concentration is expressed as a percentage of C1s signal at respective times at the take-off angle of 90º (i.e. normal to the surface). The estimated analysis depth is ~4.7 nm.

At *t* = 1440 min the concentration of Au decreases from its initial value. Angle resolved XPS analysis (**Figure 3b**) reveals, within a depth of ~1.6 to 4.7 nm from the surface, that the Au NPs

are evenly distributed beneath the air-polymer interface. This result suggests that by this stage the wetting layer already covers the particles and the NPs are pushed towards the bulk of the film. The decrease in concentration may be related to the aggregation that occurs during particle diffusion as mentioned above. However, it is also possible that some of the Au NPs diffuse below the investigation depth and, therefore, do not contribute to the XPS signal. Heating for t = 4320 min or 10080 min leads to further decreases in concentration at all measured depths. At these times the Au concentration decreases with decreasing take-off angle (or closer proximity to the surface). This confirms the NP embedding and suggests that the Au NPs are driven beyond the analysis depth of ~4.7 nm from the air-polymer interface.

In the survey spectrum at t = 1440 min (corresponding to the time the maximum roughness is measured) a Si2s signal is observed (see **Table 1**) and, given the additional increase in O1s signal at this time, we interpret these signatures as arising from the native SiO_x layer under the polymer. At t = 1440 min roughness is at its maximum observed value (**Figure 2**) arising from a well-developed pattern (**Figure 1**) of large amplitude. As a result the polymer thickness in the pattern troughs can be smaller than ~4.7 nm. Since the XPS beam size is relatively wide (700 μm x 300 μm) the signal is acquired from both peaks and troughs. Consequently, the underlying native SiO_x layer is observed. At later (heating) times, the pattern roughness decreases. Therefore, the polymer thickness in the troughs increases. As a result the SiO_x layer is no longer observed. Indeed, at t = 4320 min or 10080 min a Si signature is no longer detected in the survey spectra.

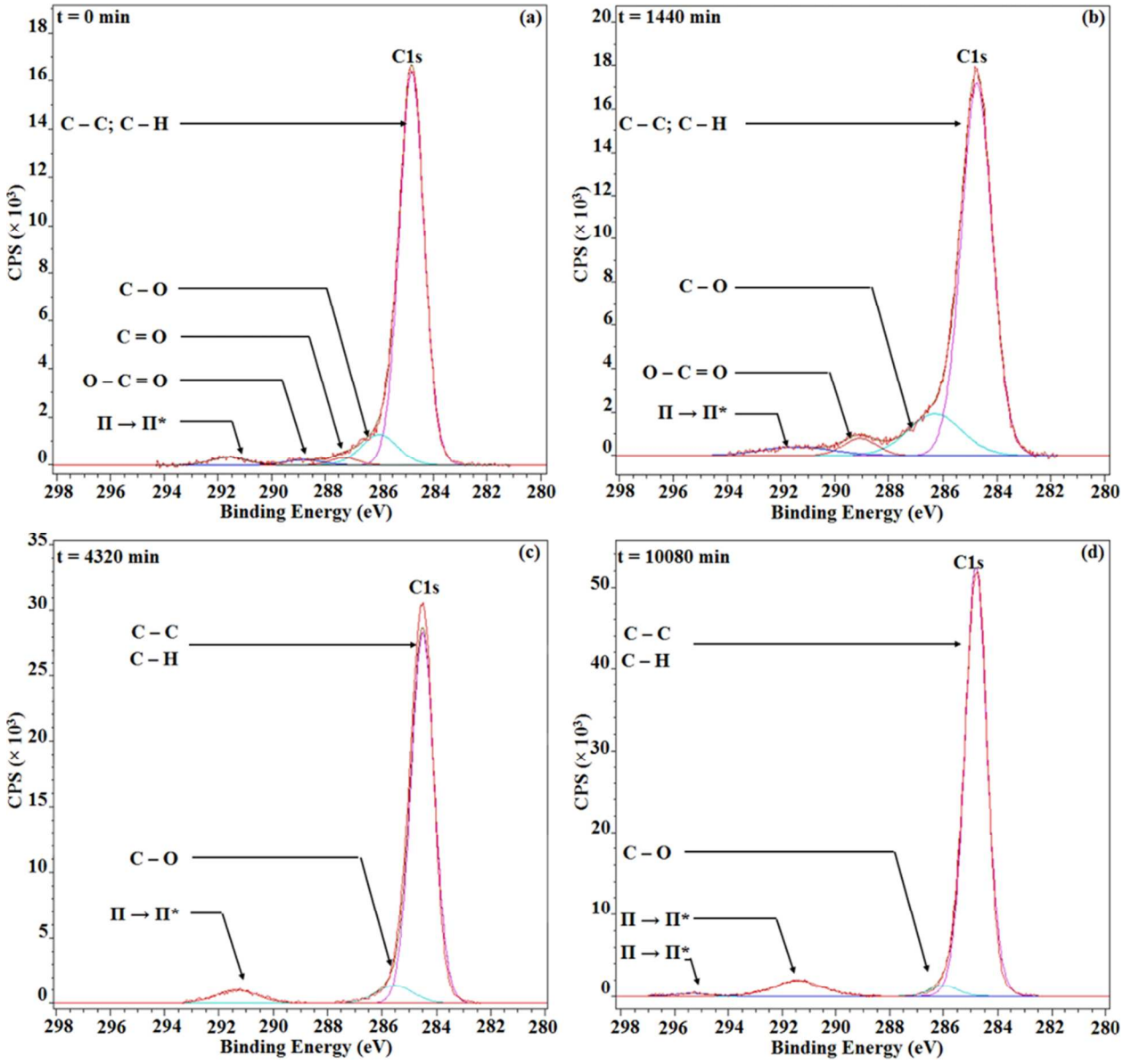

Figure 4. C1s photoelectron peaks at normal incidence (a) before (t = 0 min, h_{PS10} = 25 nm) and after heating for (b) t = 1440 min (h_{PS10} = 25 nm), (c) t = 4320 min (h_{PS10} = 26 nm) and (d) t = 10080 min (h_{PS10} = 28 nm). The shake-up Π → Π* peaks (where the second peak at 295 eV has an intensity of ~ 1/5 from the first one) represents a PS signature. The spectra were analyzed using Casa XPS software and the assignments made using NIST X-ray Photoelectron Spectroscopy Database, version 3.5. The minimum number of peaks was used for fitting the spectra.

The changes in the high resolution C1s spectrum (see **Table 2**) give information on the chemical changes that occur in the polymer film due to heating. The initial Au plasma sputter deposition leads to partial degradation of the polymer film (t = 0 min), the incorporation of oxygen, and formation of carbon-oxygen compounds. As Au embeds, the degradation increases (t = 1440 min), but at later times (t = 4320 and 10080 min), as a result of evaporation, the fraction of pristine polymer increases, as reflected by the increased intensity of the main C1s peak and (Π→Π*) shake-up satellites (**Figure 4** and **Table 2**). In fact, the effects of thermal degradation seem absent by t = 10080 min as only the pristine polystyrene signature is visible in the C1s spectrum (**Figure 4d**). Therefore, as previously reported,[18,19] thermal degradation plays only a secondary role. The pattern roughness is controlled by changes in Au NP distribution. We also note that for the studied samples (and independently of the Au NP concentration present at the polymer surface) nucleation dewetting is never observed in the Si/SiO_x/Polymer/AuNP/Air region.

DISCUSSION

In this study as embedding of NPs occur the amount of Au at the air-polymer interface decreases and this coincides with a decrease in the surface roughness. The observed pattern is induced initially by a spinodal instability in the thin film. The pattern wavelength remains constant as the surface roughness decreases and the NPs embed. Beyond an extended heating time (>37440 min), by extrapolation, the expectation is that the film becomes flat and so reaches a stable steady state. The decrease in roughness with heating time proceeds independently of chemical changes to the films as a result of their heating.

Different mechanisms can be hypothesized to explain these experimental findings. One is that the roughness reduction might be due to chemical degradation (as a result of the thermal heating in air) followed by a subsequent evaporation of the polymer. Indeed, by t = 1440 min chain scission and cross-linking may have occurred and new carbon species formed as indicated in **Table 2**. Chain scission (if significantly present) would lead to lower viscosity enhancing the growth or the decay of the pattern features; neither enhancement was experimentally observed. Continuous cross-linking might lead to increased rigidity of the film, thereby, freezing-in the pattern development. Evaporation of chemical species (like C=O present at the surface) could then lead to a thinning effect and therefore, the film roughness would decrease as observed. Such a situation might also account for a constant wavelength. However, the emergence of the Si signature in the survey spectrum (t = 1440 min) and its later disappearance indicate that the decrease in roughness is not dominated by evaporation. Otherwise more and more underlying substrate would be exposed and this signal would increase. If the polymer is significantly cross-linked, the amount of Au in the first ~4.7 nm from the surface should remain constant or only marginally reduce as the Au becomes trapped in a solidifying polymer. Neither effect is observed. On the contrary, by t = 10080 min we observe a decrease in the Au 4f, and the disappearance of the Si2s peaks. Therefore, we conclude that thermal degradation cannot play a major role in the film stabilization (by t = 10080 min at least) as it is inconsistent with the experimental findings.

The presence of a capping layer that embeds with the NPs would lead to changes in viscosity and surface tension. Such a layer may be formed due to bridges i.e. polymer chains that interconnect the Au NPs. We have shown that this bridging effect is related to the particle size and the edge-to-edge distance between the Au NPs.[18] The layer would increase the viscosity of

the upper surface and the surface tension. As the particles diffuse into the polymer film they might remain interconnected with less and less Au present in the first ~ 4.7 nm. This would lead to an embedded nanocomposite layer within the film. Consequently, the viscosity and surface tension would change. However, a change in the surface tension would lead to a change in the pattern wavelength[3,18] and this is not observed.

Another possible explanation is that the reduction in pattern roughness is a relaxation effect. Such an effect can appear once the coercive field causing the initial surface undulations is "*switched off*". A similar reduction in roughness without change in feature wavelength was reported for sinusoidal surface waves of a viscous liquid created using nano-imprinting.[27] After imprinting, heating of the polymer film above its glass transition temperature causes the amplitude of the surface wave to decay exponentially in time.[27] Here, as long as Au is present in sufficient amount at the surface the effects of the spinodal instability development are observed. As the Au particles embed a certain distance below the air-polymer interface, the coercive field cannot sustain the surface undulations, the pattern roughness diminishes and the film tends to become flat. We previously[18] found that the amount of Au measured by XPS (normal incidence) agrees with SEM surface observation. Here, by t = 1440 min, Au coverage at the air-polymer interface decreases by 50% (see **Table 1**) and no Au is seen on the polymer surface by SEM. At this point the maximum in the pattern roughness is measured (**Figure 2b**) and the presence of the SiO_x signal in the XPS spectrum indicates the pattern is well developed (see **Table 1** and earlier). However, by t = 10080 min the Au concentration decreases by ~97%, the roughness decreases by more than 50% and the SiO_x signal is absent. The roughness decrease extrapolates at later times to a flat film. Thus, the decreasing Au coverage as a result of embedding correlates with

the gradual disappearance of the pattern. This indicates that the coercive action ceases and the film is relaxing.

Reducing Au coverage can affect the instability development. In a similar Si/SiO_x/PS/AuNP/Air system, but with a thicker (h_{PS} = 44 nm) polymer layer and identical nominal Au thickness (h_{Au} = 1 nm), a spinodal instability is induced by the surface presence of Au NPs as their potential, $\Phi_{AuNP}(h_p, R_p)$, dominates the total interaction potential Φ.[16] However, as coverage reduces to ~1/3 of its initial value, the film is observed to be flat when Φ is dominated by the polymer potential Φ_{poly}. For a thicker PS film, however, no embedding occurs. The reduction in coverage is due to a surface aggregation and rearrangement process, and the pattern wavelength increases gradually. Here, in the thinner PS film, embedding is the factor driving the reduction in coverage. As the NPs embed the system changes from a Si/SiO_x/Polymer/AuNP/Air to a more complex Si/SiO_x/Polymer/Polymer-AuNP/Polymer/Air configuration. We hypothesise that embedded NPs act as a nanocomposite intermediate layer (Polymer-AuNP). Φ is then dominated only by the interaction between the Si/SiO_x/Polymer and Polymer/Air interfaces. The contribution of the intermediate interfaces are negligible.[28] Without a sufficient external field to maintain the instability the thin polymer film relaxes towards a (meta-) stable flat steady state. The relaxation process may have a large time scale as Au NPs within the polymer increase the viscosity of the film owing to the polystyrene chains adsorption to Au.[18] As a result of embedding, the total potential Φ is dominated by the stabilizing factor Φ_{poly}, and the system returns to a (meta-)stable state. This is, in fact, the natural state of thin polymers that have nanoparticles as fillers, but their presence retards nucleation dewetting.[5, 29, 30]

The stability and evolution of pristine liquid films is relatively well understood and can be described by continuous models that capture the behaviour of the film thickness profile using

gradient dynamics. Despite the existence of a well-developed theory[2,31] for pristine polymer films, an understanding of the complex liquid films that contain mixtures of polymers and nanoparticles is still at an incipient stage.[32,33] From a theoretical perspective the experimental findings presented in this study might also be captured by a system of coupled equations describing the height profile evolution of the thin liquid film and particle distribution on or within the film.[19,32,33] The total energy functional of the system is complex and will contain terms describing the van der Waals interaction between the two polymer interfaces, the interaction between the Au NPs and the underlying layers, the particle embedding and the particle-particle interaction (and their aggregation) at the surface (and/or within) the film.[19,32,33]

Such coupled equations allow for dispersion curves with single or two dominant wavelengths, but also allow a flat film solution.[19] In the this study the time evolution of the process involves a uniform and homogenous spatial distribution of the particles at the surface at $t = 0$ min. Above the polymer glass-transition temperature the film becomes liquid and the system develops a single spinodal instability. When the NPs embed the dynamics move to a stable fixed point and the system returns to a flat film state i.e. to a stable flat film solution of the coupled equations. The absence of a secondary instability mode is consistent with the absence of Marangoni forces due to variation in particle density [see Ref. 19 for details].

Based on the experimental results presented here and in our previous work,[18-19] one expects that the stability of flat film steady states depends on the particle distribution (on the surface or within the film) and on the film thickness range.[2,31] Au coverage is the determining factor as a result of either embedding, here, or aggregation, reported previously.[18-19] It is anticipated that the dynamics of a nanocomposite thin film follows a heteroclinic connection between unstable and stable solutions[2,31] of the system as the Au NP coverage decreases.

Analysis and prediction of the linear stability of a polymer film containing NPs at a given depth is non-trivial as the volume number density of the nanoparticles $\rho(\mathbf{r},t)$ (where $\boldsymbol{r} = x \cdot \hat{\imath} + y \cdot \hat{\jmath} + z \cdot \hat{k}$) should be known. This is crucial as the density $\rho(\mathbf{r},t)$ controls the total interaction potential.[19] Moreover, the presence and the development of an aggregation process (if any) within the polymer film should firstly be established as it could affect both the NP size and volume number density. In this study, only the Au depth position of NPs was determined. Therefore, to evaluate the NP size and their volume number density within the polymer further experimental studies are necessary. These will require real-time in-situ monitoring (see Ref. 11 and 12) of the surface topography and NPs. Such studies are, however, beyond the purpose of this study.

In our previous studies[18, 19] we observe that during heating the Au NPs do not embed. The reduction in coverage is solely attributed to Ostwald ripening and/or slow aggregation[18] of the Au on the polymer surface or through a cluster-cluster limited aggregation process (when the Au NPs have high mobility[19]). Here, however, in contrast to our previous study[18] the nanoparticles embed for similar initial conditions. As mentioned earlier, in both cases complete embedding is expected[17,25,26] if one considers only the $\gamma_1 > \gamma_{12} + \gamma_2$ condition. However, in thin polymer films[1,18,19] the NPs' interactions with the underlying layers have to be considered. To determine when NPs embed the free energy associated with the two possible configurations (i.e. NPs on the surface and NPs embedded in the polymer) is estimated. Embedding will be expected if its occurrence is associated with a decrease in free energy and so is thermodynamically favored (see APPENDIX).

The free energy difference Δf between a NP just above and embedded below the polymer surface is given by the following *non-dimensional* equation:

$$\Delta f = \Delta g_{poly} + \Delta g_{Si} + \Delta g_{SiOx} + R'_p H \quad (1)$$

where $R'_p = R_p / h_{poly}$ and Δg_{poly}, Δg_{Si} and Δg_{SiOx} are the energy differences between the surface and embedded NP interactions with the polymer, silicon and SiO_x substrates, respectively (see the APPENDIX for details and full derivation). $R'_p H$ is a free energy entropy term where $H \equiv h_{poly} / H_0$ and H_0 is a constant dependent on the physical properties of the polymer.

Δf is a function of R'_p and H only. H_0 is determined by the choice of polymer and fixed by the selection of a free smallness parameter ϵ. If $\Delta f < 0$ then the embedding of the particles is thermodynamically preferred; if $\Delta f > 0$ the nanoparticles will not embed (see **Figure 5**). The boundary between these preferred states will be given by $\Delta f = 0$. As seen in **Figure 5a**, for Au NPs with similar R_p, the embedding is dictated by the polymer film thickness. Thus, for the thinner polymer films presented in this paper, the particles embed as $\Delta f < 0$. For thicker polymer films the particles remain at the surface ($\Delta f > 0$) and are free to aggregate as previously described.[18] For poly(methyl methacrylate) (PMMA) films NP embedding is not expected (**Figure 5b**) and, indeed, does not occur.[17] Instead, because the particles have large mobility, they are free to aggregate through a cluster-cluster diffusion limited process and can even induce a bi-modal spinodal instability.[19]

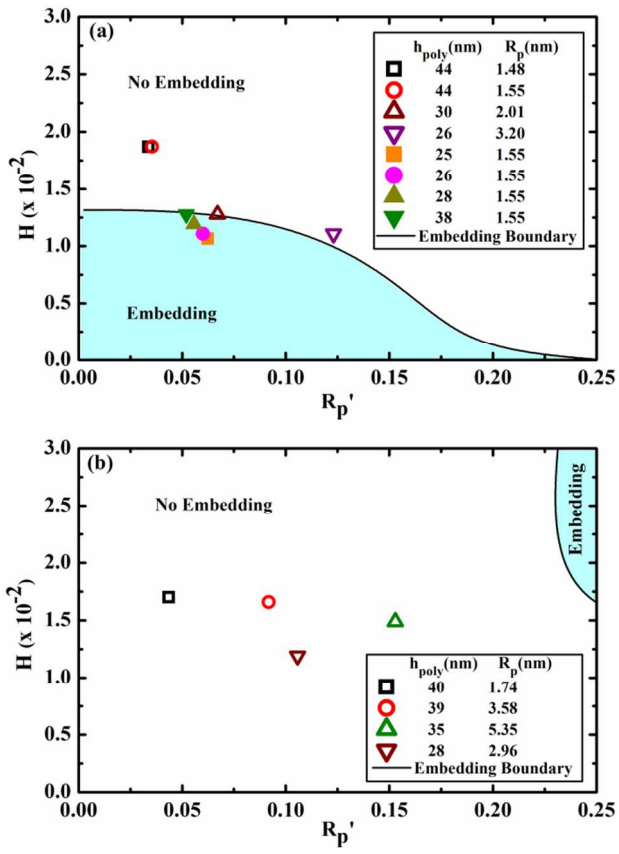

Figure 5. The embedding-phase plots of H versus R_p' for gold nanoparticles (a) on a PS film, where $a_{\mathrm{Si}} = 0.860$ and $a_{\mathrm{SiOx}} = -0.108$, and (b) on a PMMA film, where $a_{\mathrm{Si}} = 1.40$ and $a_{\mathrm{SiOx}} = 0.041$. The a_{Si} and a_{SiOx} are estimated using the calculated[18,19,28] Hamaker constants: $A_{\mathrm{Au/PS/Si}} = 9.33\cdot10^{-20}$ J, $A_{\mathrm{Au/PS/SiOx}} = -1.18\cdot10^{-20}$ J, $A_{\mathrm{Au/air/PS}} = 1.09\cdot10^{-19}$ J, $A_{\mathrm{Au/PMMA/Si}} = 1.21\cdot10^{-19}$ J, $A_{\mathrm{Au/PMMA/SiOx}} = 3.57\cdot10^{-21}$ J, $A_{\mathrm{Au/air/PMMA}} = 8.62\cdot10^{-20}$ J. Experimental samples are indicated by filled markers if particles embed and by open markers if particles do not embed. In both figures the black curve indicates where the function Δf in Eq. (A.15) goes to zero identifying where the change in the thermodynamically preferred state occurs. The shaded region shows where $\Delta f < 0$, and nanoparticle embedding is expected. The thickness of the native SiO_x layer is constant (with a value of 2 nm) and $H_0 \approx 2.35$ μm corresponding to a fitted value for $\epsilon = 3.46\cdot10^{-4}$.

CONCLUSIONS

In conclusion, we have shown, experimentally, that the stability of ultra-thin polymer films ($25 \leq h_{poly} \leq 44$ nm) to dewetting is controlled by the amount of Au NPs present at the air-polymer interface and their embedding (for $h_{poly} \leq 30$ nm). In the absence of Au NPs the film dewets by nucleation. In the presence of Au NPs a spinodal instability patterns the polymer film. As the particles embed the pattern roughness decreases while its wavelength remains constant. The effects of thermal degradation are absent by $t = 10080$ min and, therefore, thermal degradation (if present) plays a secondary role in the film flattening. Independently of the heating and cooling cycles all the samples exhibit the same dynamics: initial development of the spinodal instability pattern followed by the return to a flat film after extended heating periods. We conclude that the roughness evolution of the thin polymer is related to the amount of Au present at the air-polymer interface and its embedding. As the Au NPs embed, the dynamics of the nanocomposite thin film follows a heteroclinic connection between unstable and stable solutions. For industrial applications by tuning the duration of the heating, the roughness of the thin polymer film can be controlled. In the case of thin polymer films the embedding of the particles is determined by the change in their free energy. This depends on the nanoparticle radius, film thickness and the nanoparticle-substrate interaction. Factors such as the NP volume density and distribution (or the connectivity between the NPs through polymer chains) can play an important role when the NPs remain at the surface. Further studies are required to determine their contribution, if any, for the present case.

APPENDIX

The interaction energy between a sphere of radius R (here represented by the Au NP) and a layer of finite thickness *h* separated by a distance *d* (see **Figure 6a**) is following Tadmor *et al.*[34] given by

$$E_1 = -\frac{A_1}{6}\left[R\left(\frac{1}{d+2R} - \frac{1}{d+h+2R} - \frac{1}{d+h} + \frac{1}{d} \right) + \ln\left(\frac{d(2R+d+h)}{(d+h)(2R+d)} \right) \right] \quad \text{(A.1)}$$

where A_1 is the Hamaker constant describing the van der Waals interactions between the different media. Rescaling all depths and thicknesses in terms of a natural depth scale ξ such that $d/\xi \to d'$ and scaling the energy using the general form $\equiv 6E/A$, Equation A.1 in *non-dimensional* form becomes

$$g_1(R', d', h') = -\left[R'\left(\frac{1}{d'+2R'} - \frac{1}{d'+h'+2R'} - \frac{1}{d'+h'} + \frac{1}{d'} \right) + \ln\left(\frac{d'(2R'+d'+h')}{(d'+h')(2R'+d')} \right) \right] \quad \text{(A.2)}$$

Applying this to a Au NP above a polymer film (see **Figure 6b**), scaling all depths with the polymer thickness $\xi = h_{poly}$ such that $h_{poly} \to 1$, $R_p/h_{poly} \to R_p'$ and $\delta/h_{poly} \to \delta_p'$ and defining $A \equiv A_{Au/air/poly}$ Equation A.2 becomes

$$g_{poly} = g_1(R_p', \delta', 1) = -\left[R_p'\left(\frac{1}{\delta'+2R_p'} - \frac{1}{\delta'+1+2R_p'} - \frac{1}{\delta'+1} + \frac{1}{\delta'} \right) + \ln\left(\frac{\delta'(2R_p'+\delta'+1)}{(\delta'+1)(2R_p'+\delta')} \right) \right]$$

(A.3)

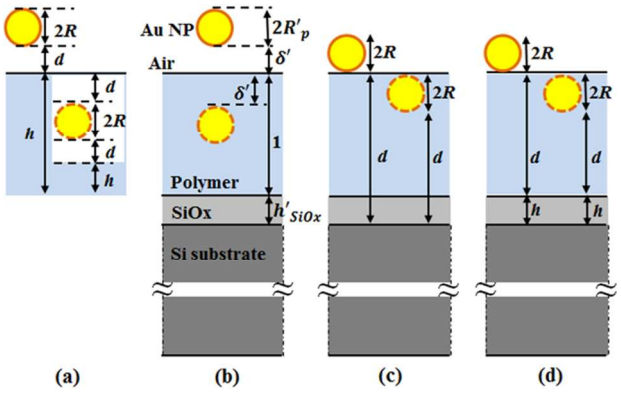

Figure 6. (a) A spherical particle above (left) and embedded in (right) a thin polymer liquid film. (b) An Au NP above and embedded within a polymer film on a Si substrate covered by its native SiO_x layer. All dimensions are scaled to the polymer film thickness h_{poly} (such scaling leads to a thickness of 1 for the thin polymer film). (c) The Au NP interaction with the Si substrate only. The presence of the native SiO_x is neglected. (d) The Au NP interaction with the native SiO_x layer. In all diagrams, the break sign in the Si substrate suggests that its thickness is much larger than the other sizes represented.

If a particle is embedded a distance d below the surface of the layer (**Figure 6a**; right) then the interactions within the top portion of the film (i.e. of thickness $2d + 2R$) are symmetric and cancel. The sphere interacts with a layer of reduced thickness as shown. For the Au NP in the polymer film $d \rightarrow \delta'$, $R \rightarrow R_p'$ (see **Figure 6b**) and the effective thickness of the film is $1-2\left(R_p'+\delta'\right)$. The interaction energy for an embedded NP is thus $g_{poly}^{e} = g_1\left(R_p', \delta', 1-2\left(R_p'+\delta'\right)\right)$ and the difference between the embedded and unembedded configurations in the limit $\delta' \rightarrow 0$ becomes

$$\Delta g_{poly} = g_{poly}^{e} - g_{poly} = \quad g_1\left(R_p', 1-2R_p'\right) - g_1\left(R_p', 1\right) \qquad \text{(A.4)}$$

The NP also interacts with the underlying Si substrate through the polymer as shown in **Figure 6c**. The thickness of the Si substrate is orders of magnitude larger than the polymer film

thickness and NP radius and, therefore, we can treat it as being semi-infinite. The interaction energy of a solid sphere of radius R with a semi-infinite wall separated by a distance d is following Tadmor *et al.* [34] given by

$$E_2(R,d) = -\frac{A_2}{6}\left[\frac{R}{d} + \frac{R}{d+2R} - \ln\left(1+2\frac{R}{d}\right)\right] \quad \text{(A.5)}$$

In non-dimensional form (see earlier) this becomes

$$g_2(R',d',a) = -a_{21}\left[\frac{R'}{d'} + \frac{R'}{d'+2R'} - \ln\left(1+2\frac{R'}{d'}\right)\right] \quad \text{(A.6)}$$

with $a_{21} = \frac{A_2}{A_1}$.

Applying Equation A.6 to a surface Au NP interacting through the polymer with the silicon substrate leads to

$$g_{Si} = g_2\left(R'_p, 1+h'_{SiOx}, a_{Si}\right) = -a_{Si}\left[\frac{R'_p}{1+h'_{SiOx}} + \frac{R'_p}{1+h'_{SiOx}+2R'_p} - \ln\left(1+2\frac{R'_p}{1+h'_{SiOx}}\right)\right] \quad \text{(A.7)}$$

where $a_{Si} = \frac{A_{Au/poly/Si}}{A_{Au/air/poly}}$ and $h_{SiOx}/h_{poly,} \rightarrow h'_{SiOx}$.

For an embedded particle $g^e_{Si} = g_2\left(R'_p, 1-2R'_p+h'_{SiOx}, a_{Si}\right)$ and using Equation A.6 the difference in interaction energy between an embedded and surface NP is

$$\Delta g_{Si} = g_2\left(R'_p, 1-2R'_p+h'_{SiOx}, a_{Si}\right) - g_2\left(R'_p, 1+h'_{SiOx}, a_{Si}\right) \quad \text{(A.8)}$$

The interaction energy of the surface NP through the polymer film with the native SiO_x layer (see **Figure 6d**) is, following Equation A.2, given by $g_{SiOx} = a_{SiOx} g_1\left(R'_p, 1, h'_{SiOx}\right)$. For the embedded NP $g^e_{SiOx} = a_{SiOx} g_1\left(R'_p, 1-2R'_p, h'_{SiOx}\right)$ where $a_{SiOx} = \frac{A_{Au/poly/SiOx}}{A_{Au/air/poly}}$. Thus, the difference in energy between the embedded and surface NP due to this interaction is given by

$$\Delta g_{SiOx} = a_{SiOx}\left(g_1\left(R'_p, 1-2R'_p, h'_{SiOx}\right) - g_1\left(R'_p, 1, h'_{SiOx}\right)\right) \quad \text{(A.9)}$$

The total interaction energy difference between the surface and embedded NP configurations is then

$$\Delta g = \Delta g_{poly} + \Delta g_{Si} + \Delta g_{SiOx} \quad \text{(A.10)}$$

The entropy difference between the at-surface and embedded NP configurations is obtained using:[25, 26]

$$\Delta S = -k_B \frac{N_p N}{V} \frac{4\pi\left(R'_p h_{poly}\right)\varepsilon b^2\left(1-\ln 2\right)}{6} \quad \text{(A.11)}$$

for a NP of radius $R_p = R'_p h_{poly}$ embedded in a polymer of degree N, with N_p polymer chains in a volume V of average length b, and where ε is a parameter (<<1) related to the increased polymer density at the NP surface. ε in this study is treated as a free parameter.

Following the scaling form used above, we write the entropy free energy term as:

$$T_0 \frac{6\Delta S}{A_{Au/air/poly}} = -R'_p H \quad \text{(A.12a)}$$

where

$$H \equiv \frac{h_{poly}}{H_0} \text{ and } H_0 = \frac{A_{Au/air/poly}}{4\pi\rho N k_B T_0 \varepsilon b^2\left(1-\ln 2\right)} \quad \text{(A.12b)}$$

Note that h'_{SiOx} can be expressed as $h'_{SiOx} = \frac{h_{SiOx}}{HH_0}$ and thus h'_{SiOx} is seen to be a function of H for constant h_{SiOx} and H_0. As the free energy of the nanoparticle is given by

$$\Delta F = \Delta E - T_0 \Delta S \quad \text{(A.13)}$$

by defining $\Delta f \equiv \frac{6\Delta F}{A_{Au/air/poly}}$, Equation A.13 can be written as

$$\Delta f = \frac{6\Delta E}{A_{Au/air/poly}} - T_0 \frac{6\Delta S}{A_{Au/air/poly}} = \Delta g + R'_p H \quad \text{(A.14)}$$

Finally using Equations A.4, A.8–A.10, and since $h'_{SiOx} \equiv h'_{SiOx}(H)$, this becomes

$$\begin{aligned}\Delta f \quad &= g_1\left(R'_p, 1-2R'_p\right) - g_1\left(R'_p, 1\right) + g_2\left(R'_p, 1-2R'_p + h'_{SiOx}(H), a_{Si}\right) - g_2\left(R'_p, 1+h'_{SiOx}(H), a_{Si}\right) \\ &+ a_{SiOx}\left(g_1\left(R'_p, 1-2R'_p, h'_{SiOx}(H)\right) - g_1\left(R'_p, 1, h'_{SiOx}(H)\right)\right) + R'_p H\end{aligned} \quad \text{(A.15)}$$

SUPPORTING INFORMATION

The ancillary material contains further details on the experimental procedure used for sample preparation and their investigation. This material is available free of charge via the Internet at http://pubs.acs.org.

AUTHOR INFORMATION

Corresponding Author

George Amarandei *Email: george.amarandei@ul.ie

Author Contributions

The manuscript was written through contributions of all authors. All authors have given approval to the final version of the manuscript.

ACKNOWLEDGMENT

We acknowledge support under EU Framework 7 for projects MRTN-CT-2004005728 (PATTERNS) and PERG04-GA-2008-239426 (POLYPATT) and from Tyndall National Institute through Science Foundation Ireland (SFI) funded National Access Programme (Project NAP 200). We thank Dr. Fathima Laffir for performing the XPS measurements and for her help in interpreting the data.

ABBREVIATIONS

PS, polystyrene; PMMA, poly(methyl methacrylate); NP, nanoparticle; XPS, X-ray photoelectron spectroscopy.

REFERENCES

(1) Seemann, R.; Herminghaus, S.; Jacobs, K. Dewetting Patterns and Molecular Forces: A Reconciliation. *Phys. Rev. Lett.* **2001**, *86*, 5534–5537.

(2) Reiter, G. Dewetting of Thin Polymer Films. *Phys. Rev. Lett.* **1992**, *68*, 75–78.

(3) Thiele, U. In *Thin films of Soft Matter*; Kalliadasis, S., Thiele, U., Eds.; Springer, Wien, 2007; Chapter Structure formation in thin liquid films, pp. 25–93.

(4) Mukherjee, R.; Das, S.; Das, A.; Sharma, S. K.; Raychaudhuri, A. K.; Sharma, A. Stability and Dewetting of Metal Nanoparticle Filled Thin Polymer Films: Control of Instability Length Scale and Dynamics. *ACS Nano* **2010**, *4*, 3709–3724.

(5) Wong, H. C.; Cabral, J. T. Mechanism and Kinetics of Fullerene Association in Polystyrene Thin Film Mixtures. *Macromolecules* **2011**, *44*, 4530–4537.

(6) Jia, X.; Listak, J.; Witherspoon, V.; Kalu, E. E.; Yang, X.; Bockstaller, M. R. Effect of Matrix Molecular Weight on the Coarsening Mechanism of Polymer-Grafted Gold Nanocrystals. *Langmuir* **2010**, *26*, 12190–12197.

(7) Buxton G. A.; Clarke N. Stress-guided self-assembly in Dutcher films. *Phys. Rev. E* **2006**, *74*, 041807.

(8) Dalnoki-Veress, K.; Nickel, B. G.; Dutcher, J. R. Dispersion-Driven Morphology of Mechanically Confined Polymer Films. *Phys. Rev. Lett.* 1999, *82*, 1486–1489.

(9) Yoo, P. J.; Suh, K. Y.; Kang, H.; Lee, H. H. Polymer Elasticity-Driven Wrinkling and Coarsening in High Temperature Buckling of Metal-Capped Polymer Thin Films. *Phys. Rev. Lett.* **2004**, *93*, 034301.

(10) Al-Hussein, M.; Schindler, M.; Ruderer, M. A.; Perlich, J.; Schwartzkopf, M.; Herzog, G.; Heidmann, B.; Buffet, A.; Roth, S. V.; Müller-Buschbaum, P. In Situ X‐ray Study of the Structural Evolution of Gold Nano-Domains by Spray Deposition on Thin Conductive P3HT Films. *Langmuir* **2013**, *29*, 2490−2497.

(11) Kaune, G.; Ruderer, M. A.; Metwalli, E.; Wang, W.; Couet, S.; Schlage, K.; Röhlsberger, R.; Roth, S. V.; Müller-Buschbaum, P. In Situ GISAXS Study of Gold Film Growth on Conducting Polymer Films. *ACS. Appl. Mater. Interfaces* **2009**, *1*, 353−360.

(12) Roth, S. V.; Herzog, G.; Körstgens, V.; Buffet, A.; Schwartzkopf, M.; Perlich, J.; Abul Kashem, M. M.; Döhrmann, R.; Gehrke, R.; Rothkirch, A.; Stassig, A.; Wurth, W.; Benecke, G.; Li, C.; Fratzl, P.; Rawolle, M.; Müller-Buschbaum, P. In Situ Observation of Cluster Formation During Nanoparticle Solution Casting on a Colloidal Film. *J. Phys.: Condens. Matter* **2011**, *23*, 254208.

(13) Susrutha, B.; Ram, S.; Tyagi, A. K. Effects of Gold Nanoparticles on Rheology of Nanofluids Containing Poly(vinylidene fluoride) Molecules. *J. Nanofluids* 2012, *1*, 120–127.

(14) Phule, A. D.; Ram, S.; Tyagi, A. K. Anchoring Silver with Poly(vinylidene fluoride) Molecules in Model Flocculates and Its Effects on Rheology in Stable Nanofluids. *J. Nanofluids* **2013**, *2*, 249–260.

(15) Faupel, F.; Zaporojtchenko, V.; Strunskus, T.; Elbahri, M. Metal-Polymer Nanocomposites for Functional Applications. *Adv. Eng. Mater.* **2010**, *12*, 1177−1190.

(16) Schwartzkopf, M.; Buffet, A.; Körstgens, V.; Metwalli, E.; Schlage, K.; Benecke, G.; Perlich, J.; Rawolle, M.; Rothkirch, A.; Heidmann, B.; Herzog, G.; Müller-Buschbaum, P.; Röhlsberger, R.; Gehrke, R.; Stribeck, N.; Roth, S. V. From Atoms to Layers: In Situ Gold Cluster Growth Kinetics During Sputter Deposition. *Nanoscale* **2013**, *5*, 5053−5062.

(17) Deshmukh, R. D.; Composto R. J. Direct Observation of Nanoparticle Embedding into the Surface of a Polymer Melt. *Langmuir* **2007**, *23*, 13169–13173.

(18) Amarandei, G.; O'Dwyer, C.; Arshak A.; D. Corcoran. The Stability of Thin Polymer Films as Controlled by Changes in Uniformly Sputtered Gold. *Soft Matter* **2013**, 9, 2695–2702.

(19) Amarandei, G.; O'Dwyer, C.; Arshak, A.; Thiele, U.; Steiner U.; Corcoran D. Effect of Au Nanoparticle Spatial Distribution on the Stability of Thin Polymer Films. *Langmuir* **2013**, *29*, 6706–6714.

(20) Kunz M. Z.; Shull, K. R.; Kellock, A. J. Morphologies of Discontinuous Gold Films on Amorphous Polymer Substrates *J. Appl. Phys.* 1992, *72*, 4458–4460.

(21) Smithson, R. L. W.; McClure, D. J.; Evans, D. F. Effects of Polymer Substrate Surface Energy on Nucleation and Growth of Evaporated Gold Films. *Thin Solid Films* **1997**, *307*, 110 – 112.

(22) Erichsen, J.; Kanzow, J.; Schürmann, U.; Dolgner, K.; Günther-Schade, K.; Strunskus, T.; Zaporojtchenko, V.; Faupel, F. Investigation of the Surface Glass Transition Temperature by

Embedding of Noble Metal Nanoclusters into Monodisperse Polystyrenes. *Macromolecules* **2004**, *37*, 1831–1838.

(23) Teichroeb J. H.; Forrest, J. A. Direct Imaging of Nanoparticle Embedding to Probe Viscoelasticity of Polymer Surfaces. *Phys. Rev. Lett.* **2003**, *91*, 016104.

(24) Sharp, J. S.; Teichroeb J. H.; Forrest, J. A. The Properties of Free Polymer Surfaces and Their Influence on the Glass Transition Temperature of Thin Polystyrene Films. *Eur. Phys. J. E: Soft Matter.* **2004**, *15*, 473–487.

(25) Kovacs, G. J.; Vincett, P. S. Formation and Thermodynamic Stability of a Novel Class of Useful Materials: Close-Packed Monolayers of Submicron Monodisperse Spheres Just below a Polymer Surface. *J. Colloid Interface Sci.* **1982**, 90, 335–351.

(26) Kovacs, G. J.; Vincett, P. S. Subsurface Particle Monolayer and Film Formation in Softenable Substrates: Techniques and Thermodynamic Criteria. *Thin Solid Films* **1984**, *111*, 65–81.

(27) Peng, H. G.; Kong, Y. P.; Yee, A. F. Relaxation Kinetics of Nanostructures on Polymer Surface: Effect of Stress, Chain Mobility, and Spatial Confinement. *Macromolecules* **2010**, *43*, 409–417.

(28) Israelachvili, J. N. *Intermolecular and Surface Forces*, 2nd ed; Academic Press: London, 1992.

(29) Barnes, K.A.; Karim, A.; Douglas, J. F.; Nakatani, A. I.; Gruell, H.; Amis, E. J. Suppression of Dewetting in Nanoparticle-Filled Polymer Films. *Macromolecules* **2000**, *33*, 4177–4185.

(30) Krishnan, R. S.; Mackay, M. E.; Duxbury, P. M.; Hawker, C. J.; Asokan, S.; Wong, M. S.; Goyette, R.; Thiyagarajan, P. Improved Polymer Thin-Film Wetting Behavior Through Nanoparticle Segregation to Interfaces. *J. Phys.: Condens. Matter* **2007**, 19, 356003.

(31) Thiele, U.; Velarde, M. G.; Neuffer, K.; Pomeau, Y. Film Rupture in the Diffuse Interface Model Coupled to Hydrodynamics. *Phys. Rev. E.* **2001**, 64, 031602.

(32) Thiele, U.; Teodorova, D. V.; Lopez, H. Gradient Dynamics Description for Films of Mixtures and Suspensions: Dewetting Triggered by Coupled Film Height and Concentration Fluctuations. *Phys. Rev. Lett.* **2013**, *111*, 117801.

(33) Thiele, U.; Archer, A. J.; Plapp, M. Thermodynamically Consistent Description of the Hydrodynamics of Free Surfaces Covered by Insoluble Surfactants of High Concentration. *Phys. Fluids* **2012**, *24*, 102107.

(34) Tadmor, R. The London–van der Waals Interaction Energy Between Objects of Various Geometries. *J. Phys.: Condens. Matter* **2001**, *13*, L195–L202.

TOC

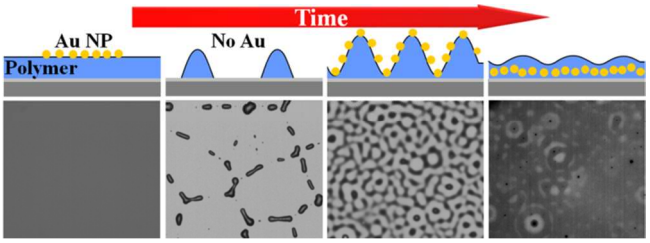

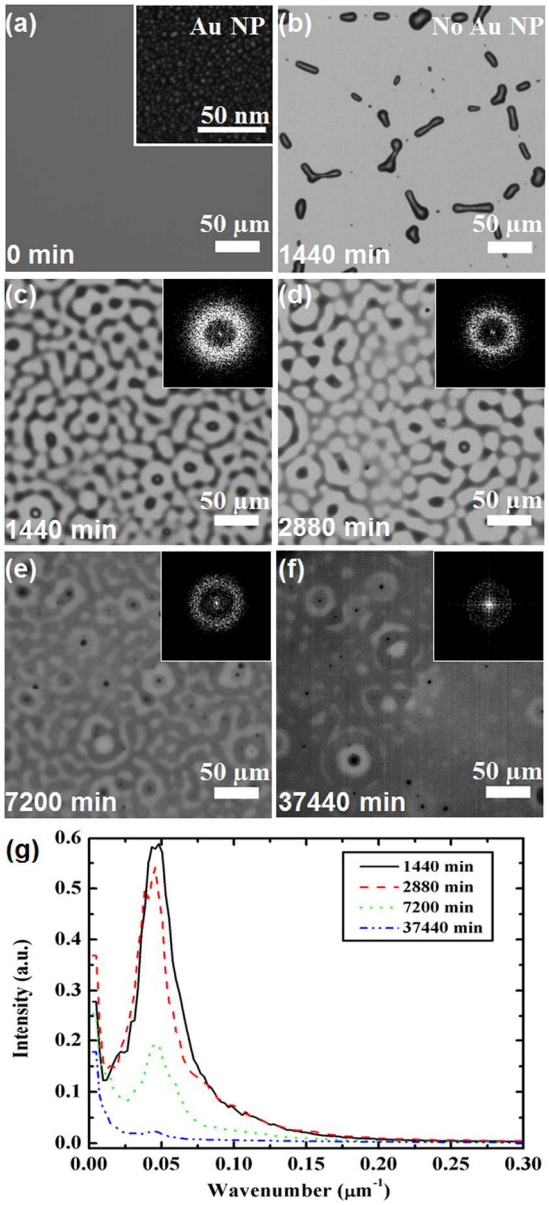

184x406mm (300 x 300 DPI)

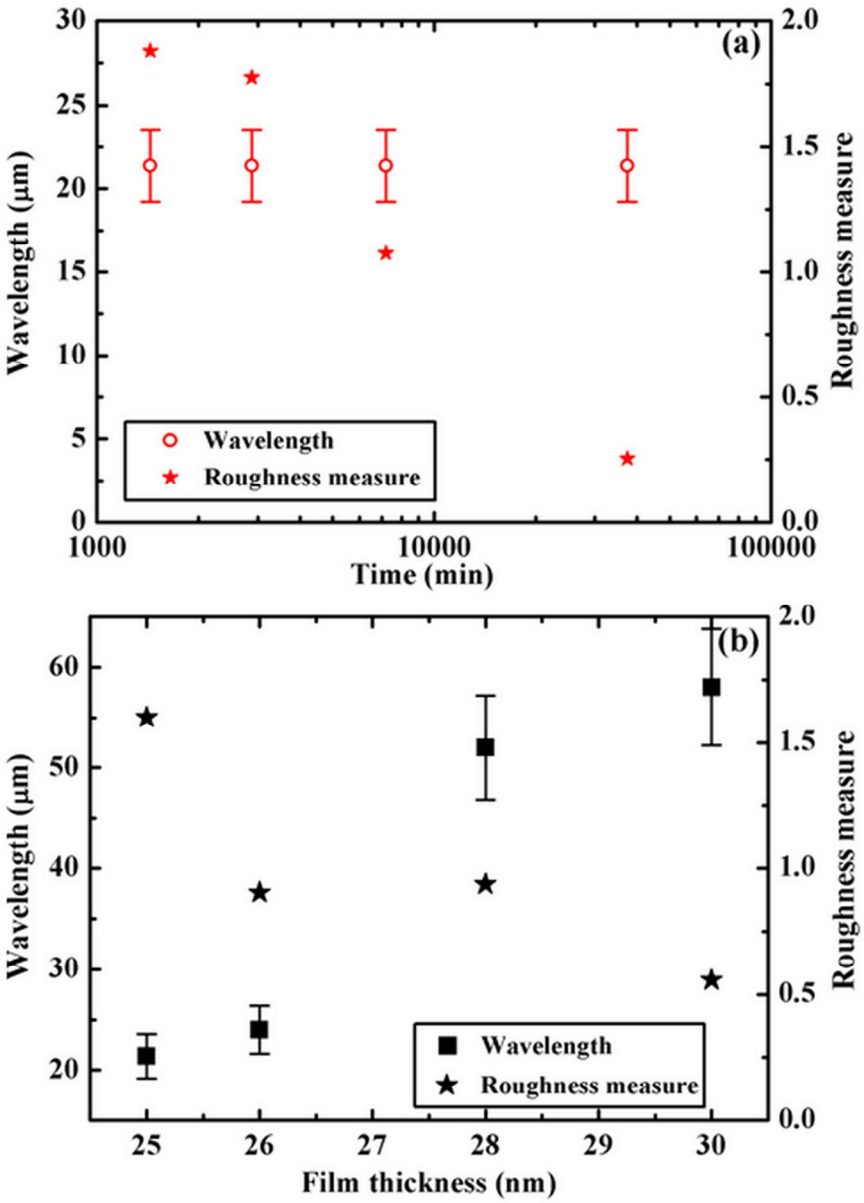

81x112mm (300 x 300 DPI)

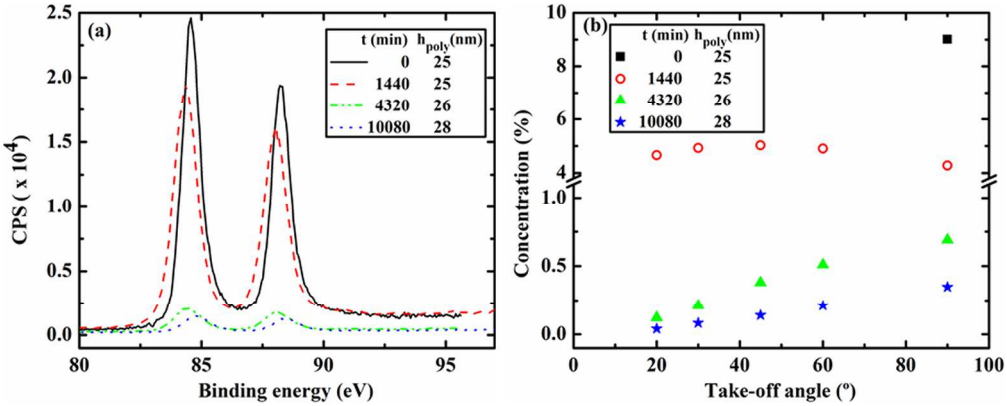

694x278mm (300 x 300 DPI)

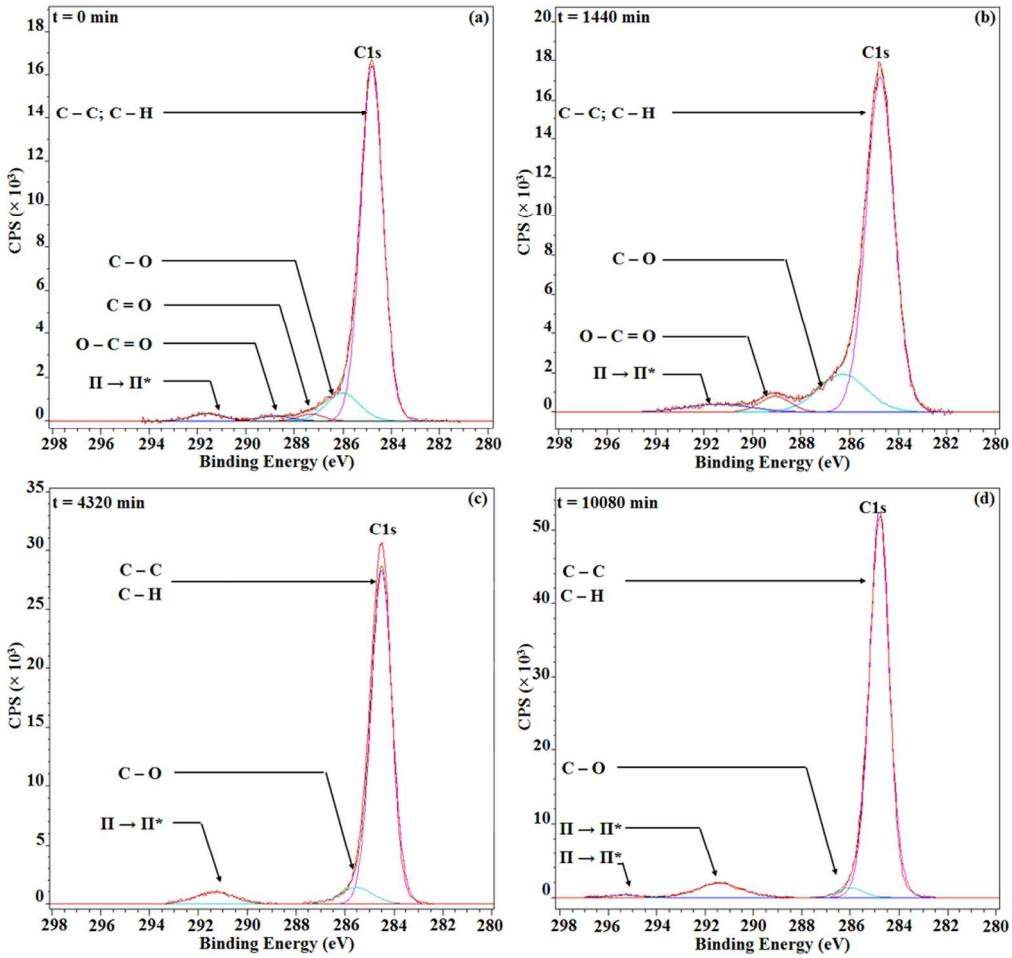

215x204mm (300 x 300 DPI)

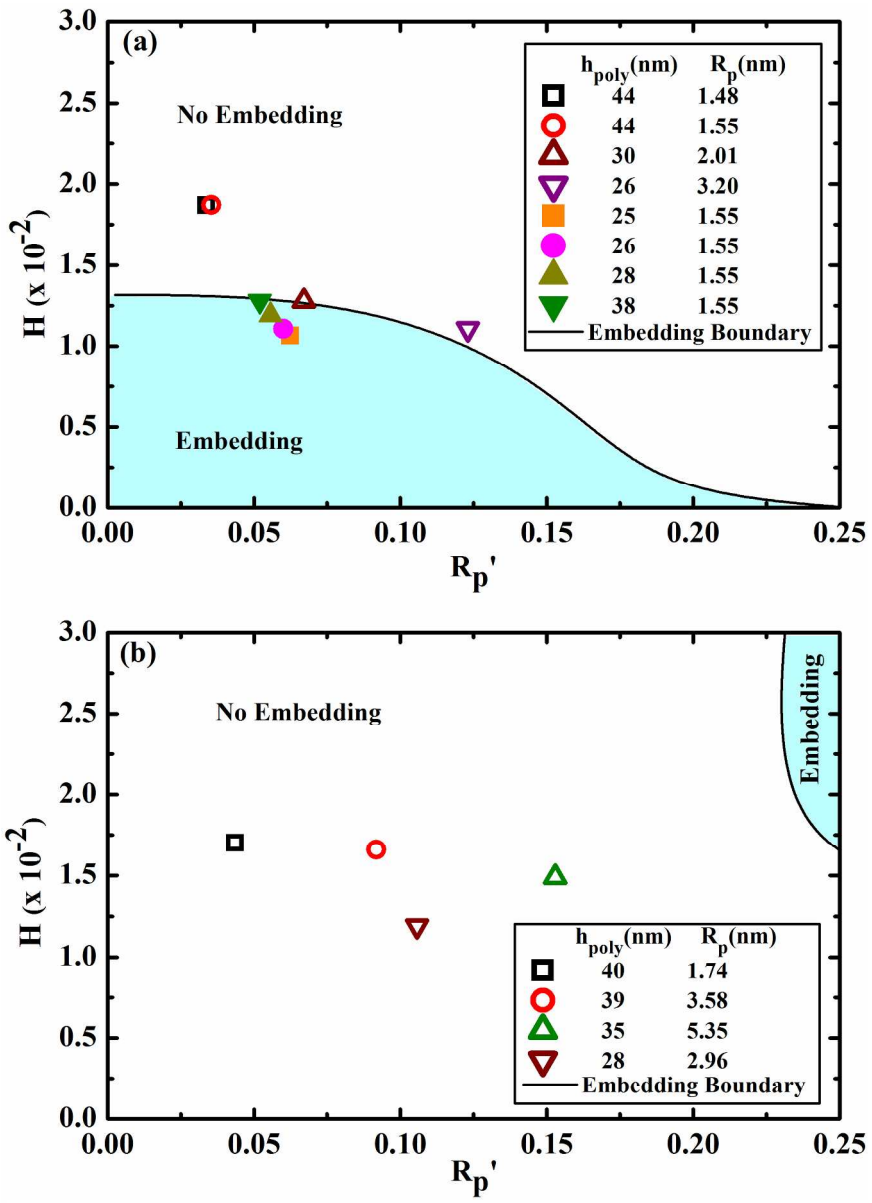

272x377mm (300 x 300 DPI)

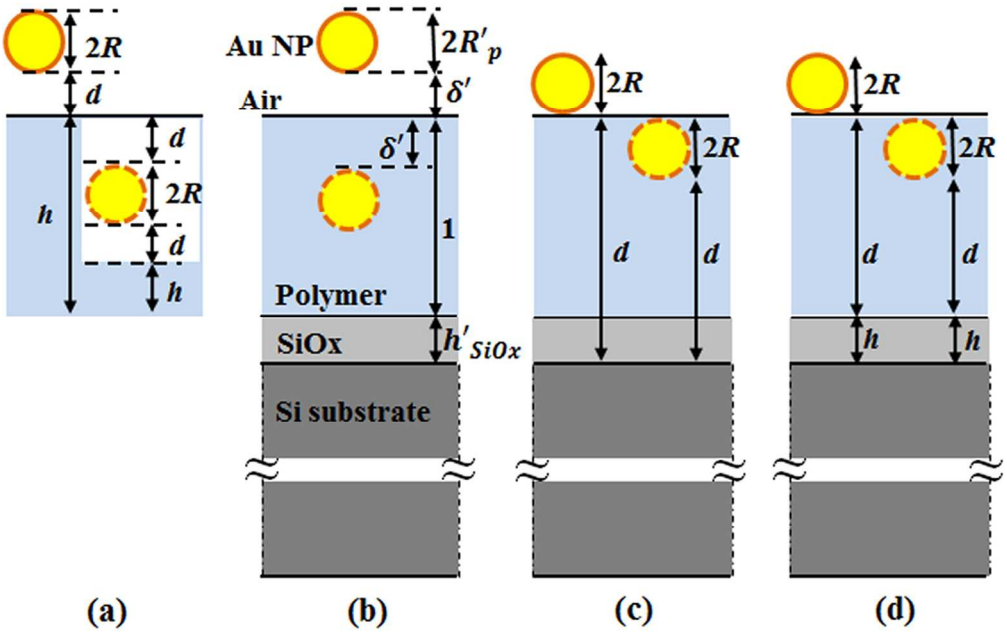

171x107mm (300 x 300 DPI)

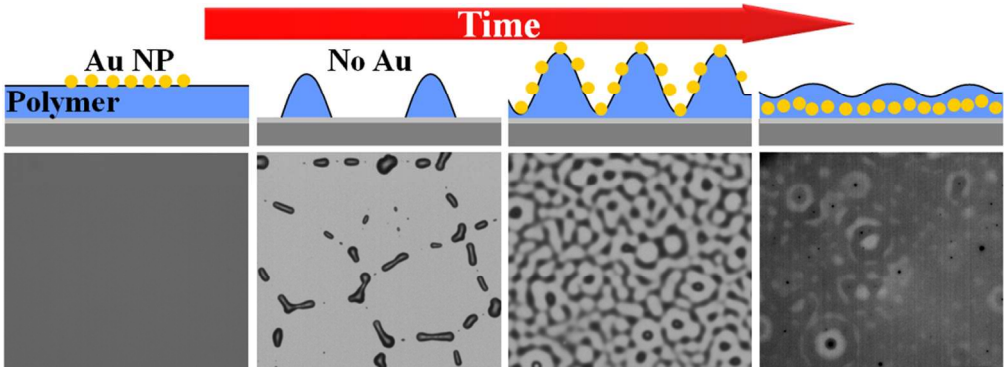

216x78mm (300 x 300 DPI)

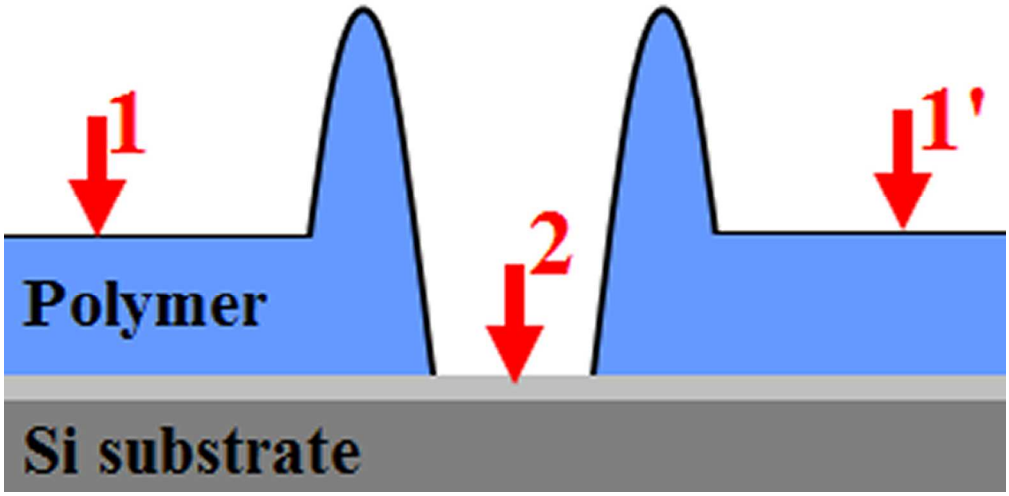

215x105mm (300 x 300 DPI)

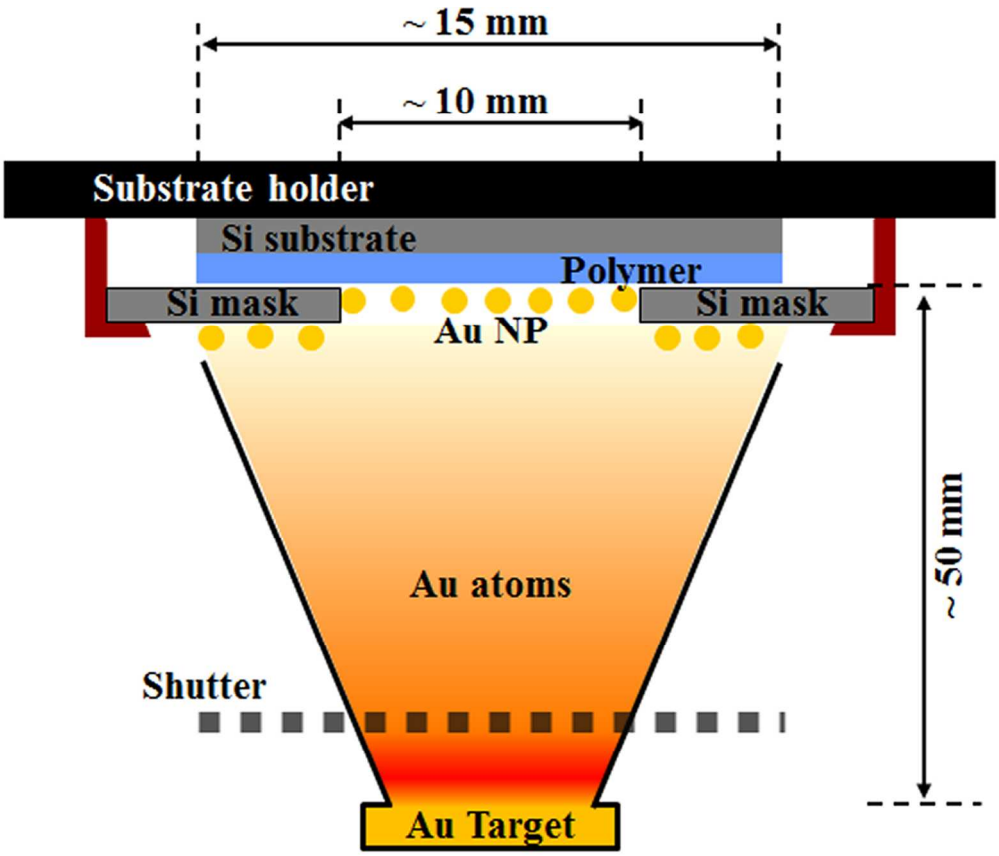

140x119mm (300 x 300 DPI)